SUPPLEMENTARY MATERIAL

Sensitive radio-frequency read-out of quantum dots using an ultra-low-noise SQUID amplifier

F. J. Schupp[1,†], F. Vigneau[1,†], Y. Wen[1], A. Mavalankar[1], J. Griffiths[2], G. A. C. Jones[2], I. Farrer[2,3], D. A. Ritchie[2], C. G. Smith[2], L. C. Camenzind[4], L. Yu[4], D. M. Zumbühl[4], G. A. D. Briggs[1], N. Ares[1], and E. A. Laird[1,5*]

[1] *University of Oxford, Department of Materials, 16 Parks Road, Oxford OX1 3PH, UK*

[2] *Cavendish Laboratory, J.J. Thomson Avenue, Cambridge CB3 0HE, UK*

[3] *Department of Electronic and Electrical Engineering, University of Sheffield, Sheffield S1 3JD, UK*

[4] *Department of Physics, University of Basel, 4056 Basel, Switzerland*

[5] *Department of Physics, University of Lancaster, Lancaster, LA1 4YB, United Kingdom*

(Dated: May 21, 2020)

CONTENTS

S1. CHARGE SENSITIVITY AND QUBIT READOUT

Two distinct kinds of charge sensitivity are important in radio-frequency charge sensing, and both values are quantified in the main text. Here we clarify the difference between the two and explain how they are estimated.

A. Sensitivity to oscillating charge $S_{\tilde{Q}}$

Dispersive readout of a singlet-triplet qubit measures the effective quantum capacitance C_q that arises when an electron oscillates between two quantum dots [S1–S5]. The circuit is sensitive to the oscillating charge $\tilde{Q}$ on a nearby electrode. In order to distinguish singlet and triplet states, the sensitivity should be good enough to resolve the signal due to a single oscillating electron within the qubit relaxation time.

The sensitivity to oscillating charge $S_{\tilde{Q}}$ is related to the capacitance sensitivity S_C by

$$S_{\tilde{Q}} = \sqrt{2} V_0 S_C \tag{S1}$$

where V_0 is the root-mean-square RF voltage on the capacitor electrode. This follows from the fact that the amplitude of the charge oscillation on the electrode is $\tilde{Q} = \sqrt{2} V_0 C$. While Eq. (S1) suggests that the sensitivity could be improved without limit by increasing the injected RF voltage, this will not happen because the quantum capacitance of the singlet-triplet qubit exists only near zero voltage bias [S1]. To estimate the readout time, it is therefore necessary to average the quantum capacitance $C_\mathrm{q}(V)$ over an entire RF cycle [S5], i.e. to calculate

$$\overline{C_\mathrm{q}} = \frac{1}{2\sqrt{2}V_0} \int_{-\sqrt{2}V_0}^{\sqrt{2}V_0} C_\mathrm{q}(V) \mathrm{d}V \tag{S2}$$

where V is the instantaneous voltage on the gate electrode. The bandwidth for detecting this capacitance with unit SNR is then

$$\Delta f = (\overline{C_\mathrm{q}}/S_C)^2. \tag{S3}$$

In a double quantum dot, the quantum capacitance of the singlet state is:

$$C_\mathrm{q}(V) = (e\lambda)^2 \frac{(2t)^2}{2\left((\lambda e V)^2 + (2t)^2\right)^{3/2}} \tag{S4}$$

* e.a.laird@lancaster.ac.uk
† these authors contributed equally to this work

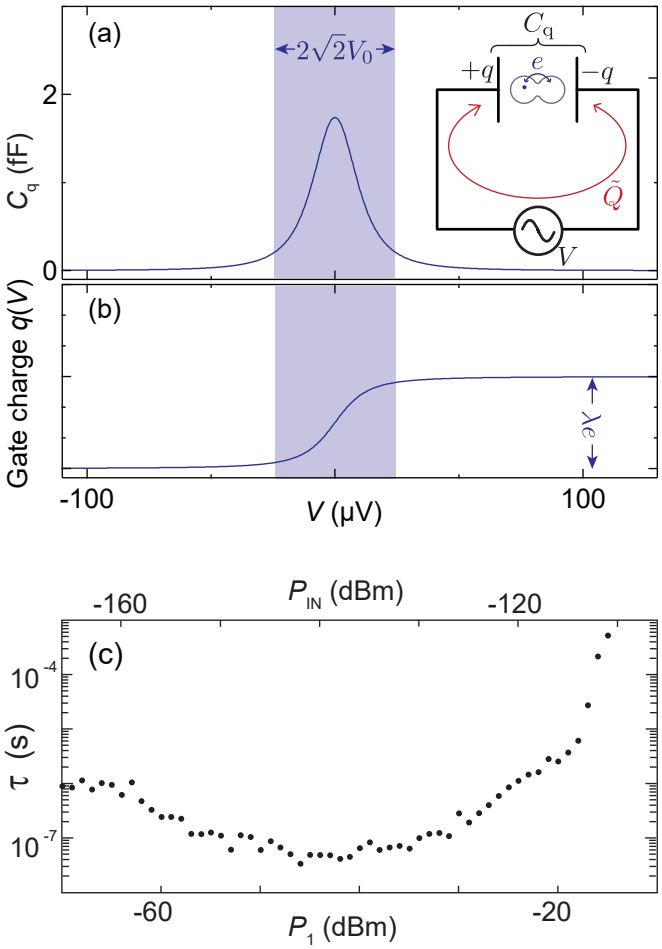

FIG. S1. Sensitivity to oscillating charge (a) Quantum capacitance of a double quantum dot as a function of voltage on the coupling electrode, from Eq. (S4). Inset cartoon: arrangement of drive voltage V, quantum capacitance C_q, instantaneous electrode charge q, and oscillating component of the electrode charge $\tilde{Q}$. (b) Charge on the coupling electrode, which acts as one plate of the capacitor. The shaded region is the range of an RF cycle over which the integral Eq. (S2) is calculated. (c) Read-out time $\tau = 1/2\Delta f$, estimated from Eq. (S3) and Fig. 4 of the main text. These data are plotted as a function of input power P_1 into port 1 (bottom axis) and of the corresponding power P_{IN} at the SQUID input (top axis).

where t is the inter-dot tunnel coupling and λ is the lever arm relating V to the detuning between the two dots. In a typical device [S1], $t = h \times 500$ MHz and $\lambda = 0.3$. This capacitance is plotted in Fig. S1(a), and the corresponding electrode charge $q(V)$ in Fig. S1(b).

To maximise the signal, the drive amplitude V_0 should be set larger than the peak width in Fig. S1(b). Equation (S2) then simplifies to

$$\overline{C_Q} = \frac{\lambda e}{2\sqrt{2}V_0} \tag{S5}$$

and the read-out bandwidth is:

$$\Delta f = \left(\frac{\lambda e}{2\sqrt{2}\,V_0 S_C}\right)^2 = \left(\frac{\lambda e}{2S_{\tilde{Q}}}\right)^2. \tag{S6}$$

To optimise the sensitivity, λ should be maximised while the product $V_0 S_C$ is minimised.

In this experiment, V_0 is limited not just by the width of the capacitance peak but also by the saturation threshold of the SQUID. Assuming the parameters from the device in Ref. [S1], the condition that the drive voltage exceeds the capacitance peak width, i.e. $V_0 \gtrsim t/\lambda e$, is reached around $P_1 = -31$ dBm in our setup. From the data in Fig. 2(e) of the main text we do not expect an increased SQUID amplifier noise until an input power of $P_{IN} = -120$ dBm (or P_1 around -27 dBm depending on the matching of the quantum dot device). The dynamic range of our setup is therefore sufficient for the device from Ref. [S1]. Devices with a larger lever arm $\lambda > 0.3$ are likely to require less input power to the SQUID amplifier, and therefore the dynamic range should not limit the circuit performance.

We can calculate the required read-out time for each value of V_0 (and thus P_1), by numerically integrating Eq. (S2) and substituting into Eq. (S3), using the values S_C measured in Fig. 4 of the main text. The read-out time is then given by $\tau = 1/2\Delta f$. The calculated values for the device from Ref. [S1], plotted in Fig. S1(c), reach an optimal value of $\tau = 26$ ns, implying that this singlet-triplet qubit could be read out in a single shot.

B. Sensitivity to quasi-static charge S_Q

In an electrometer configuration, the RF circuit detects a quasi-static charge Q via the resulting shift of a Coulomb peak. This is the configuration that is used when a charge sensing single-electron transistor (SET) is used for qubit readout [S6–S11]. In this configuration, the charge sensitivity, denoted S_Q, can be characterized in two ways. One way, used in Section V of the main paper, uses a gate voltage pulse to induce a large change ΔQ, on the order of one electron charge, to the equilibrium charge of the quantum dot device. As stated in the main paper, the estimated sensitivity in this case is

$$S_{\Delta Q} = e\sqrt{\tau_{\min}} \tag{S7}$$

where $\tau_{\min}$ is the measurement time that allows the change in device impedance to be resolved.

The other way to characterize the sensitivity is to modulate the gate voltage so as to induce a small charge δQ, and to measure the resulting sidebands that appear in the spectrum of the reflected signal. The sensitivity in this case is (analogous to Eq. 3 of the main text)

$$S_{\delta Q} = \frac{\delta Q}{\sqrt{2\Delta f}} 10^{-\mathrm{SNR}/20} \tag{S8}$$

where Δf is the measurement bandwidth and $\delta Q = e\,\delta V_L/\Delta V_{CB}$ is the induced charge variation on the quantum dot as a result of the gate modulation (in our measurement the left gate in Fig. 1 of the main text). Here ΔV_{CB} is the Coulomb peak spacing and δV_L is the gate modulation. In general $S_{\delta Q} \leq S_{\Delta Q}$.

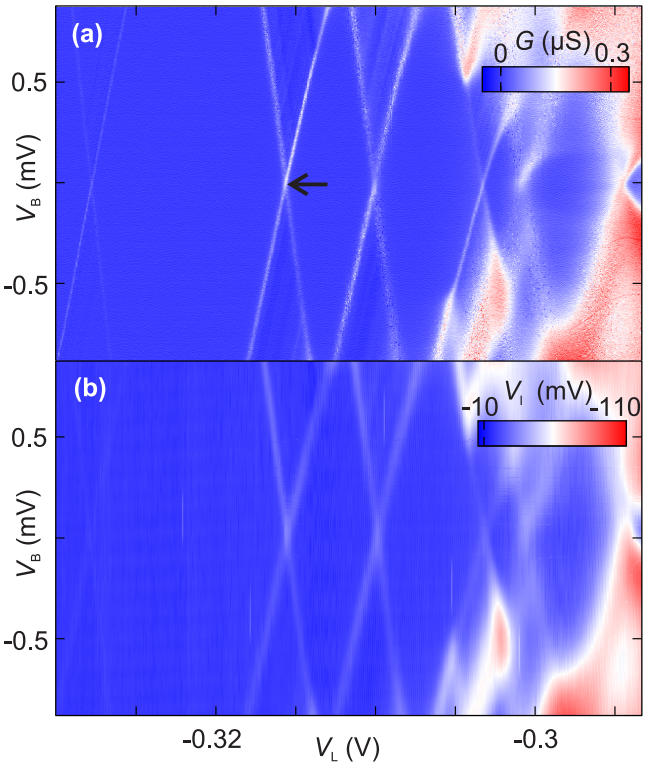

FIG. S2. Measurement of the single quantum dot device used in Section II-IV of the main text, in order to evaluate the sensitivity of a charge sensor. (a) Conductance G as a function of gate voltage V_L and bias voltage V_B. The black arrow indicates the Coulomb peak where the charge sensitivity was measured. (b) I quadrature, measured by homodyne detection (as in Fig. 1 of the main text) over the same range.

S2. CHARGE SENSING USING A SINGLE QUANTUM DOT

Here we measure again the single quantum dot device used in Section II-IV of the main text in order to operate this device as an electrometer for quasi-static charge.

A. Configuring the quantum dot as a single-electron transistor

To operate the quantum dot as an SET, we adjust the gate voltages to configure the quantum dot's tunnel barriers into the Coulomb blockade regime. We first measure the charge stability diagram at DC and at RF. Figure S2(a) shows the DC conductance G as a function of gate voltage V_L and source-drain bias voltage V_B while Fig. S2(b) shows the corresponding output voltage V_D of the RF detection circuit. Both measurements clearly show the Coulomb diamonds characteristic of single-electron transport [S12]. On the flank of a Coulomb peak, the dot's conductance and capacitance depend sharply on the electrochemical potential, making it a sensitive detector for electrical signals.

B. Measuring and optimising the charge sensitivity

To measure the charge sensitivity $S_{\delta Q}$, we center the gate voltage on the flank of a Coulomb peak ($V_\mathrm{L} = -315.56$ mV, black arrow in Fig. S2(a)). Modulating the gate voltage while measuring the power spectrum of the reflected signal, we use Eq. (S8) to infer $S_{\delta\mathrm{Q}}$.

The charge sensitivity is optimized in the same way as the capacitance sensitivity in the main text. In this section and in Figs. 2-6 we show how to optimize successively with respect to gate voltage V_L, varactor tuning voltage V_S, RF excitation P_1, and gate modulation amplitude δV_L. The aim is to operate on the flank of a Coulomb peak, where the change in sample impedance is maximized for a small gate voltage modulation. The ideal Coulomb peak is as sharp as possible in gate voltage and the peak conductivity is high. To find the most suitable Coulomb peak we begin the optimization by measuring the sensitivity $S_{\delta Q}$ as a function of gate voltage (Figure S3). As expected, the sensitivity is best on the flanks of the Coulomb peaks (compare Fig. 5 in the main text). The δQ used in Eq. (S8) is calculated taking account of the different Coulomb peak spacing in Fig. S3. The best sensitivity with these parameters is $S_{\delta\mathrm{Q}} = 295\,\mu e/\sqrt{\mathrm{Hz}}$ at a gate voltage of $V_\mathrm{L} = -315.6\,\mathrm{mV}$ (green marker in Fig. S3).

Next we optimize the sensitivity with respect to varactor voltage V_S (Fig. S4). In this measurement, we adjust the carrier frequency to the best matching point at each value of V_S. We find a sensitivity of $S_{\delta\mathrm{Q}} = 182\,\mu e/\sqrt{\mathrm{Hz}}$ at $V_\mathrm{S} = 6.1\,\mathrm{V}$ and $f_\mathrm{C} = 194.56\,\mathrm{MHz}$ (green marker in Fig. S4).

Figure S5 shows the optimization with respect to input power P_1 at port 1. As in Fig. 4 of the main text, the sensitivity improves with increasing signal, until it approaches the saturation threshold of the SQUID. The slightly different power dependence compared with Fig. 4 may result from the different impedance match condition. The best charge sensitivity $S_{\delta\mathrm{Q}} = 93\,\mu e/\sqrt{\mathrm{Hz}}$ is measured at $P_1 = -26\,\mathrm{dBm}$ (green marker in Fig. S5).

Figure S6 shows the optimization of the sensitivity with respect to the amplitude δV_L. The sensitivity degrades slightly with increasing modulation amplitude because small non-linearities in the circuit (such as nonlinear device transconductance) scatter signal power into higher sidebands that are not measured. The best sensitivity in Figure S6 is $S_{\delta\mathrm{Q}} = 80\,\mu e/\sqrt{\mathrm{Hz}}$ measured at the lowest modulation amplitude $\delta V_\mathrm{L} = 12\,\mu\mathrm{V_{rms}}$. At even lower modulation amplitude, the signal becomes difficult to distinguish from external interference.

Finally we re-optimize the measurement with respect to gate voltage, holding other parameters at their optimal settings (Fig. S7). The final optimized sensitivity is $S_{\delta Q} = 60 \pm 20\,\mu e/\sqrt{\mathrm{Hz}}$ at $V_\mathrm{L} = -315.556\,\mathrm{mV}$. The associated power spectrum is shown in Fig. S8. This value of $S_{\delta Q}$ is about 27 times better than the previously achieved charge sensitivity in the same setup without the SQUID amplifier [S5].

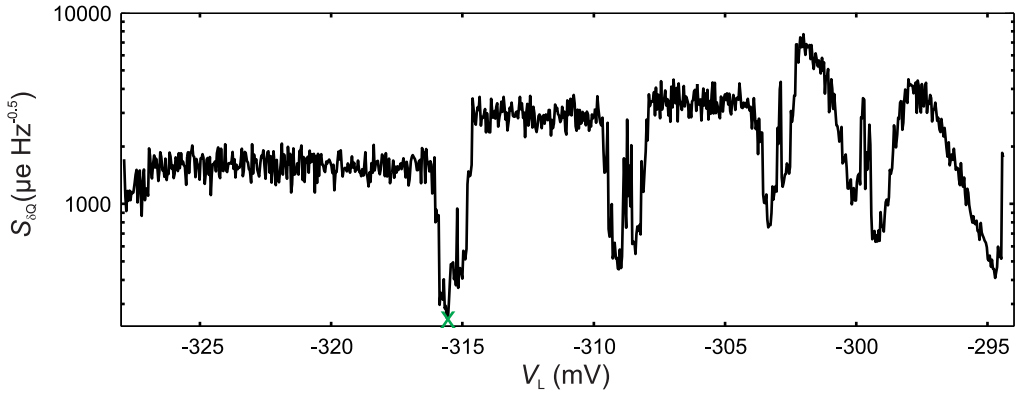

FIG. S3. Charge sensitivity $S_{\delta Q}$ as a function of gate voltage V_L at $f_C = 197\,\text{MHz}$, $V_S = 7\,\text{V}$, $f_M = 6\,\text{kHz}$, $\delta V_L = 117.8\,\mu\text{V}_{\text{rms}}$ and $P_1 = -38\,\text{dBm}$. The chosen gate voltage for further measurements $V_L = -315.6\,\text{mV}$ is indicated by the green marker.

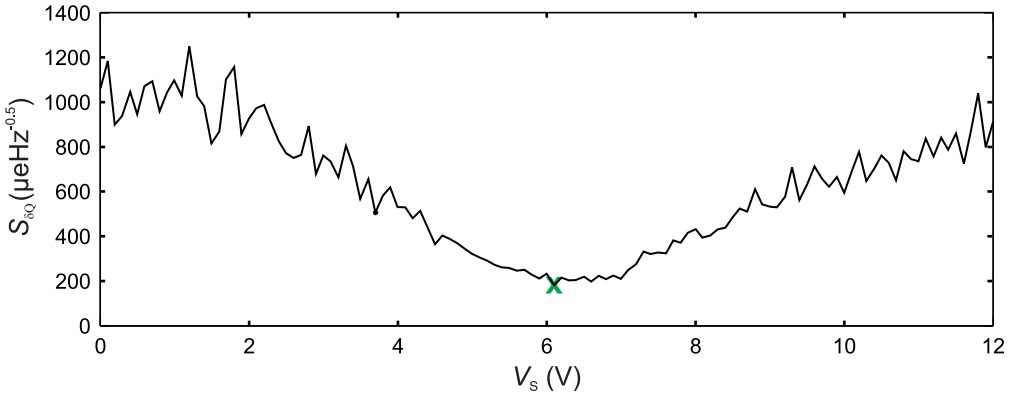

FIG. S4. Charge sensitivity $S_{\delta Q}$ as a function of varactor voltage V_S at $V_L = -315.6\,\text{mV}$, $f_M = 6\,\text{kHz}$, $\delta V_L = 117.8\,\mu\text{V}_{\text{rms}}$ and $P_1 = -38\,\text{dBm}$. The chosen varactor voltage for further measurements $V_S = 6.1\,\text{V}$ is indicated with the green marker. The associated carrier frequency is $f_C = 194.56\,\text{MHz}$.

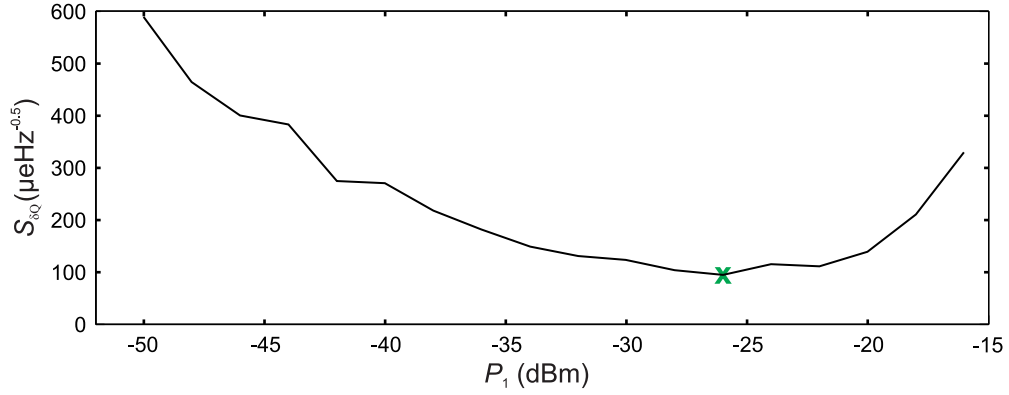

FIG. S5. Charge sensitivity $S_{\delta Q}$ as a function of power into port 1 P_1 at $V_L = -315.6\,\text{mV}$, $f_C = 194.56\,\text{MHz}$, $V_S = 6.1\,\text{V}$, $f_M = 6\,\text{kHz}$ and $\delta V_L = 117.8\,\mu\text{V}_{\text{rms}}$. The chosen $P_1 = -26\,\text{dBm}$ for further measurements is indicated by the green marker.

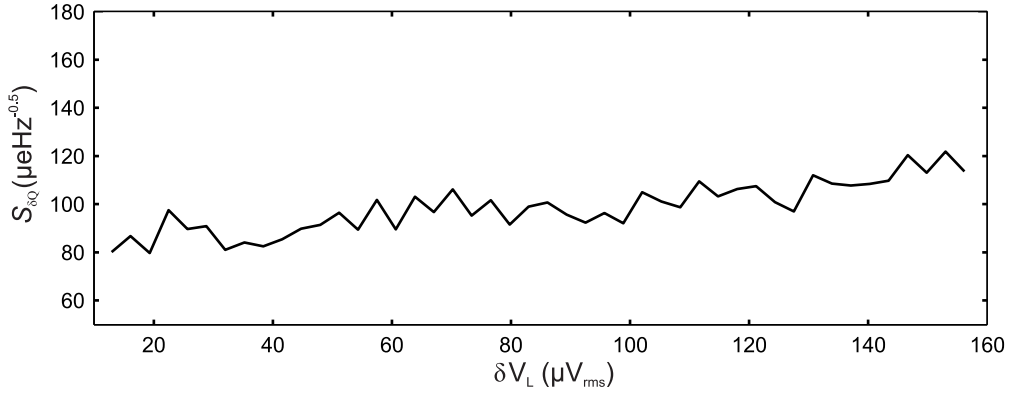

FIG. S6. Charge sensitivity $S_{\delta \mathrm{Q}}$ as a function of gate modulation amplitude δV_{L} at $V_{\mathrm{L}} = -315.6\,\mathrm{mV}$, $f_{\mathrm{C}} = 194.56\,\mathrm{MHz}$, $V_{\mathrm{S}} = 6.1\,\mathrm{V}$, $f_{\mathrm{M}} = 6\,\mathrm{kHz}$ and $P_1 = -26\,\mathrm{dBm}$. The best sensitivity is $S_{\delta \mathrm{Q}} \approx 80\,\mu e/\sqrt{\mathrm{Hz}}$.

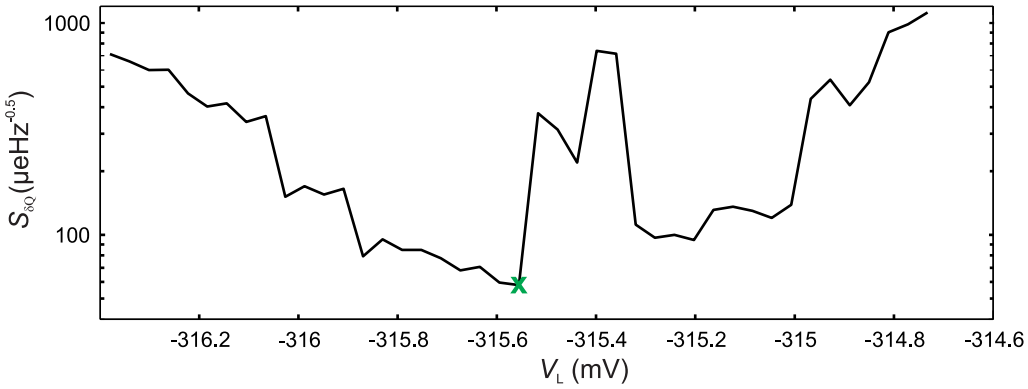

FIG. S7. Charge sensitivity $S_{\delta Q}$ as a function of gate voltage V_{L} at $\delta V_{\mathrm{L}} = 15.7\,\mu\mathrm{V_{rms}}$, $f_{\mathrm{C}} = 194.56\,\mathrm{MHz}$, $V_{\mathrm{S}} = 6.1\,\mathrm{V}$, $f_{\mathrm{M}} = 3\,\mathrm{kHz}$ and $P_1 = -26\,\mathrm{dBm}$. The best sensitivity, indicated with the green marker, is $S_{\delta Q} = 60 \pm 20\,\mu e/\sqrt{\mathrm{Hz}}$

.

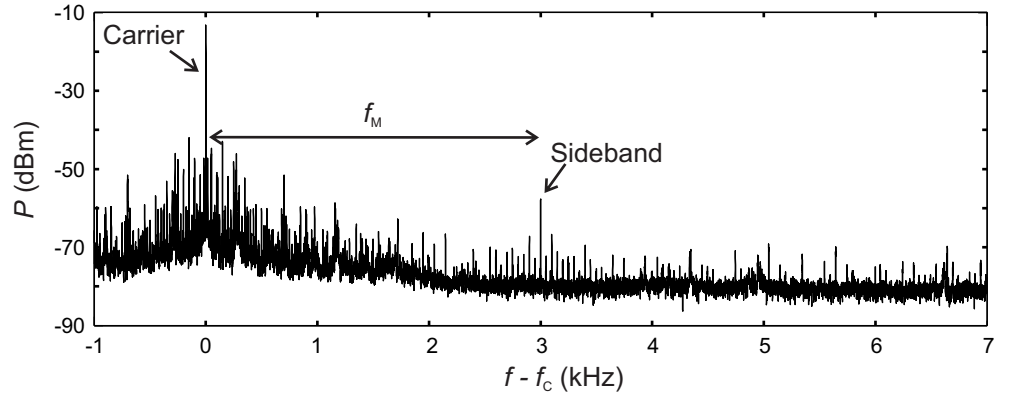

FIG. S8. Reflected power spectrum (after amplifier chain including room temperature amplifiers) in the sideband experiment for the best observed charge sensitivity in Fig. S7. The gate voltage setting is $V_{\mathrm{L}} = -315.556\,\mathrm{mV}$, as marked by the green cross in Fig. S7. The main spectral peak is the carrier tone, the marked peak is the modulation sideband, and the smaller peaks are residual interference signals.

For comparison, the best reported charge sensitivity in a semiconductor device, $S_{\delta Q} = 1.3\,\mu e/\sqrt{\text{Hz}}$ [S13], was measured using gate-based sensing, while the best reported value for reflectometry on the source contact is $S_{\delta Q} = 7.2\,\mu e/\sqrt{\text{Hz}}$ [S14]. Our charge sensitivity is therefore within one order of magnitude of the best reported values. Optimal charge sensitivity requires a small device resistance on the Coulomb peak [S15]. Whereas Ref. [S14] used a device with resistance on the Coulomb peak of 55 kΩ, the resistance in our device is 6.7 MΩ [S14, S15]. We therefore conclude that the charge sensitivity in our setup is limited by the device resistance and could be further improved with an optimized device, for which the tunnel barriers could be tuned to higher conductance while remaining within the Coulomb blockade regime.

S3. SQUID AMPLIFIER PERFORMANCE IN PREVIOUS COOLDOWN

Figure S9 shows the SQUID performance measured in a previous cooldown (before the cooldown in which the data from the main text was taken). In this measurement, the power was not yet optimized, which accounts for the elevated noise temperature of 800 mK, consistent with the power dependence in Fig. 2(e) of the main text. We also find that the optimal gain in Fig. S9(b) does not produce the lowest noise temperature in Fig. S9(d). This behaviour was previously linked to increased current noise close to the highest gain [S16].

Note that the critical current in this measurement is 12.9 µA at $I_\Phi = 0$. This is more than 2 µA higher than in Fig. 2(a) of the main text and presumably indicates a trapped flux. We have chosen $I_B = 13.1\,\mu A$ here and in the main text, in order to surpass the critical current regardless of flux.

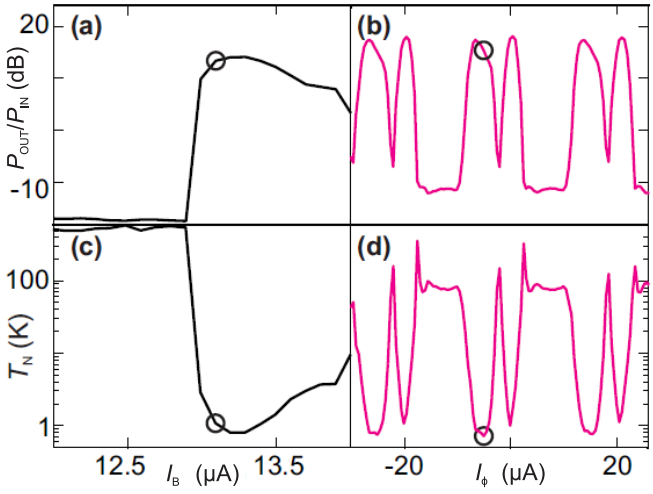

FIG. S9. SQUID amplifier performance in a previous cooldown and at a higher power $P_3 = -76$ dB.

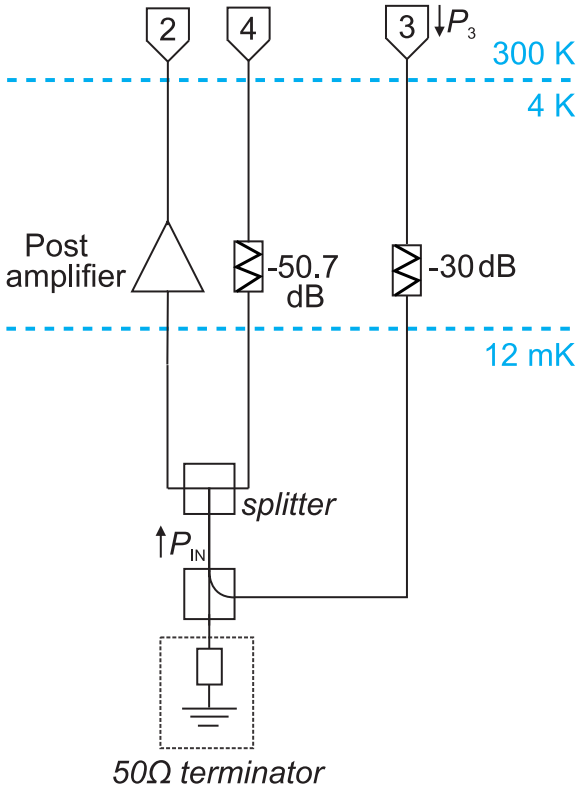

FIG. S10. Schematic of the line calibration measurement.

S4. DETAILS OF MEASUREMENT CALIBRATION

A. Determining the capacitance modulation δC

This section explains how to calculate the capacitance modulation δC, used in Eq. (3) of the main paper, from the known voltage modulation V_M across the varactor. From simulations and previous experiments [S5] with the same circuit and sample we know that the tank circuit behaves approximately as an LC resonator, whose resonance frequency is:

$$f_0(V_S) \approx \frac{1}{2\pi\sqrt{LC(V_S)}} \tag{S9}$$

where $L = 223$ nH is the inductor value and $C(V_S)$ is the capacitance as a function of varactor voltage. We can then infer the capacitance modulation δC from the voltage modulation V_M:

$$\delta C = \left|\frac{dC}{dV_S}\right| V_M = \frac{V_M}{2\pi^2 L f_0^3}\left|\frac{df_0}{dV_S}\right|. \tag{S10}$$

The measurements of Fig. 3 in the main text are used to extract the resonance frequency f_0 as a function of varactor voltage V_S and hence calculate $\frac{df_0}{dV_S}$ and δC.

B. Calibrating the input power to the amplifier chain

To measure the gain of the amplifier chain in our setup, we require a well-calibrated input power. The gain can then be determined by comparing the input and output power of the amplifier chain. Knowing this gain, together with the noise level at port 2, we can infer the noise level at the input of the SQUID amplifier.

To inject a known input power, we must know precisely the insertion loss of the input line from port 3. Although this insertion loss was confirmed at room temperature, we must further check it at low temperature to guard against small thermal variations in the cryogenic attenuators or other components. To do this, we introduce another line, entering the cryostat via port 4 (see Fig. S10), which allows the power entering the amplifier chain to be measured. The attenuation of the input line (i.e. via port 3) was now measured at base temperature in a dedicated cooldown, using the circuit shown in Fig. S10. In this measurement the tank circuit was replaced by a $50\,\Omega$ terminator on one side of the directional coupler. On the other side, the circuit was connected to a three-way symmetric resistive splitter that splits the signal equally into two lines: the RF measurement line (without the SQUID amplifier) and an additional line containing only attenuators. We know the low-temperature attenuation from the splitter to port 4, $|S_{4,\mathrm{sp}}|$, with a small error of $\pm 0.5\,\mathrm{dB}$, because this line was previously characterized in a simple transmission measurement in which it was driven through a nominally identical line. Assuming symmetry, the line attenuation is simply half the attenuation through the combined path. The symmetry of the resistive splitter was verified at room temperature.

We extract the gain in the RF measurement line $|S_{\mathrm{sp},2}|$ from the measurements of:

$$|S_{23}| = |S_{\mathrm{sp},3}| + \Delta + |S_{2,\mathrm{sp}}| \tag{S11}$$

and

$$|S_{43}| = |S_{\mathrm{sp},3}| + \Delta + |S_{4,\mathrm{sp}}| \tag{S12}$$

where Δ is the insertion loss of the splitter, and all quantities are expressed in dB. These two equations yield for the gain of the postamplifier line

$$|S_{2,\mathrm{sp}}| = |S_{23}| - |S_{43}| + |S_{4,\mathrm{sp}}| \tag{S13}$$

$$= 32 \pm 0.7\,\mathrm{dB} \tag{S14}$$

This value is in agreement with the specified gain of the postamplifier $34\pm2\,\mathrm{dB}$ taking account of a potential small loss in the rest of the measurement line.

We now extract $|S_{\mathrm{sp},3}|$, the insertion loss of the input line. To do this, we first infer the splitter loss by measuring the transmission S_{24}. Using the known attenuation $|S_{4,\mathrm{sp}}|$ and gain $|S_{2,\mathrm{sp}}|$, we extract $\Delta = |S_{24}| - |S_{\mathrm{sp},4}| - |S_{2,\mathrm{sp}}| = -6.1\,\mathrm{dB}$, close to the expected value for a three-way-symmetric resistive splitter. This value of Δ is then substituted into Eq. (S11) to infer an input insertion loss of $|S_{\mathrm{sp},3}| = 49.7\pm0.8\,\mathrm{dB}$, which agrees well with the expected losses from the inline attenuators (30 dB) and the directional coupler (20 dB). This is the value used when calculating the amplifier input power in the main text.

S5. INSTRUCTIONS FOR AMPLIFIER INSTALLATION AND TUNING

This section includes summary instructions from EZ-SQUID for installing and wiring the amplifier, a protocol for switching on the amplifier and a rough estimate of the expected dynamic range. By permission of EZ-SQUID, we have also provided their entire manual as Supplementary Material.

The original installation instructions from EZ-SQUID are:

As the bias resistors of the amplifier have only low resistance, you should add higher-value resistors at 4 K, say 100 kΩ for both currents. Connecting the amplifier directly to a room-temperature current source will couple too much noise to the SQUID. Also, if you want to measure gain, there must be at least 20 dB (30 dB would be better) of attenuation between the input of the amplifier and the room-temperature RF generator. It would also be good to decouple the output of the amplifier from the room-temperature network or spectrum analyzer by a post amplifier with sufficient gain. RF from the local oscillator of the network or spectrum analyzer coupled back into the output of the amplifier might saturate the SQUID otherwise. Finally, wireless LAN can also saturate the amplifier if the bias leads will pick up RF.

In the setup from the main text, the DC lines are filtered using an array of RC filters at the mixing chamber (total inline resistance 5.36 kΩ, total capacitance 330 pF, with Minicircuits LFCNxx RF filters and a printed circuit board meander embedded in copper powder). The RF input lines have at least 30 dB of attenuation and the output line is connected to the postamplifier sitting at 4 K. For thermalization, we wrap the amplifier in copper braid around the SMA connectors under the shield and clamp the copper braid to the mixing-chamber plate. In the future, the thermalization could be improved with a dedicated holder and shielding.

After installation and cooldown, we recommend the protocol following Sec. III of the main text:

1. Sweep current bias while monitoring the transmission through the amplifier. The critical part in this step is choosing an input power that produces signal above the noise level of the measurement when the amplifier transmission increases above the critical current. At the same time, the input power should not saturate the amplifier. As a rule of thumb, the maximum input power can be estimated by using half of the critical current as the maximum output swing. For a critical current of 10 μA and

a SQUID impedance of 15 Ω, this corresponds to a power at the output around −64 dBm. A good guess for an input power would then depend on the expected amplification. For the amplifiers in the main text with a gain around 12 dB (which might be underestimated due to reflections on the amplifier input), we should then easily be in the linear regime with a power on the input below −100 dBm. It is advisable, however, to choose the lowest possible power as the exact gain and the extent of other saturating effects (such as thermal excitations) are unknown.

2. Fix the bias current above the critical current, where you should see increased transmission in the sweep from step 1. Since the critical current depends on the flux bias, it is advisable to leave a few μA margin between the critical current and the chosen bias current to account for trapped flux. Once the bias current is fixed, sweep the flux bias current optimizing the gain in the transmission measurement. If the gain is not a smooth function as a function of flux bias around the highest gain, the bias current might be too small or the input power too high, such that you have reached the compression regime. Another reason could be noise in the bias current or flux.

3. Choose a flux bias associated with optimized performance and characterize the amplifier as needed for the experiment. This can include a measurement of the dynamic range as in Fig. 3(e) of the main text or a frequency sweep. Note that the input impedance, and therefore the dynamic range, depends on frequency.

[S1] K. D. Petersson, C. G. Smith, D. Anderson, P. Atkinson, G. A. C. Jones, and D. A. Ritchie, Nano Letters **10**, 2789 (2010).

[S2] J. Colless, A. Mahoney, J. Hornibrook, A. Doherty, H. Lu, A. Gossard, and D. Reilly, Physical Review Letters **110**, 046805 (2013).

[S3] J. Verduijn, M. Vinet, and S. Rogge, Applied Physics Letters **104**, 102107 (2014).

[S4] M. F. Gonzalez-Zalba, S. Barraud, A. J. Ferguson, and A. C. Betz, Nature Communications **2**, 1 (2015).

[S5] N. Ares, F. J. Schupp, A. Mavalankar, G. Rogers, J. Griffiths, G. A. C. Jones, I. Farrer, D. A. Ritchie, C. G. Smith, A. Cottet, G. A. D. Briggs, and E. A. Laird, Physical Review Applied **5**, 034011 (2016).

[S6] R. J. Schoelkopf, Science **280**, 1238 (1998).

[S7] J. M. Elzerman, R. Hanson, J. S. Greidanus, L. H. Willems van Beveren, S. De Franceschi, L. M. K. Vandersypen, S. Tarucha, and L. P. Kouwenhoven, Physical Review B **67**, 161308 (2003).

[S8] J. R. Petta, A. C. Johnson, J. M. Taylor, E. A. Laird, A. Yacoby, M. D. Lukin, C. M. Marcus, M. P. Hanson, and A. C. Gossard, Science **309**, 2180 (2005).

[S9] D. J. Reilly, C. M. Marcus, M. P. Hanson, and A. C. Gossard, Applied Physics Letters **91**, 162101 (2007).

[S10] M. C. Cassidy, A. S. Dzurak, R. G. Clark, K. D. Petersson, I. Farrer, D. A. Ritchie, and C. G. Smith, Applied Physics Letters **91**, 6 (2007).

[S11] C. Barthel, D. J. Reilly, C. M. Marcus, M. P. Hanson, and A. C. Gossard, Physical Review Letters **103**, 160503 (2009).

[S12] R. Hanson, L. P. Kouwenhoven, J. R. Petta, S. Tarucha, and L. M. K. Vandersypen, Reviews of Modern Physics **79**, 1217 (2007).

[S13] I. Ahmed, J. A. Haigh, S. Schaal, S. Barraud, Y. Zhu, C.-m. Lee, M. Amado, J. W. A. Robinson, A. Rossi, J. J. L. Morton, and M. F. Gonzalez-Zalba, Physical Review Applied **10**, 014018 (2018).

[S14] S. J. Angus, A. J. Ferguson, A. S. Dzurak, and R. G. Clark, Applied Physics Letters **92**, 112103 (2008).

[S15] A. N. Korotkov and M. A. Paalanen, Applied Physics Letters **4052**, 3 (1999).

[S16] B. Schmidt and M. Mück, Applied Physics Letters **100**, 152601 (2012).